Molecular Design of Efficient Chlorine- and Carboxylate-Functionalized Donor Polymers for Nonfullerene Organic Solar Cells Enabling Processing with Eco-Friendly Solvent in Air

Sung Jae Jeon, Young Hoon Kim, Dong Hyun Hong, Nam Gyu Yang, Yong Woon Han, and Doo Kyung Moon

Realizing the commercial applications of nonfullerene organic solar cells (NFOSCs) require a balanced of power conversion efficiency (PCE), production cost, and stability. However, because most high-performance NFOSC devices contain air-sensitive donor polymers that have low solubility in eco-friendly solvents, their fabrication requires halogenated solvents and an inert atmosphere. Herein, an air-processed inverted NFOSC device is developed using a relatively cost-effective chlorine- and carboxylate-functionalized bithiophene-based donor polymer, P(F-BiT)-COOBOCl(out). When blended with 3,9-bis(2-methylene-((3-(1,1-dicyanomethylene)-6,7-difluoro)-indanone))-5,5,11,11-tetrakis(4-hexylphenyl)-dithieno[2,3-*d*:2′,3′-*d*′]-*s*-indaceno[1,2-*b*:5,6-*b*′] dithiophene (IT-4F), the resultant device yields a high PCE of 11.91%, with good shelf-life stability and photostability under ambient conditions without encapsulation, and less performance degradation than most reported NFOSCs. Importantly, when the polymer blend is processed in air with an eco-friendly solvent, 1,2,4-trimethylbenzene, the resultant device exhibits a reasonably high PCE of 10.60% (certified PCE: 10.467%) without encapsulation, which is the highest value reported to date for NFOSCs fabricated under such conditions. The potential of this high-performance and eco-friendly processable polymer is further demonstrated in the excellent PCE of 14.22% of a device with a P(F-BiT)-COOBOCl(out):Y6-BO-4Cl blend prepared in *o*-xylene solvent. This study provides perspectives and opportunities for designing and developing efficient photoactive materials as a new strategy for the commercialization of NFOSCs.

Dr. S. J. Jeon, Y. H. Kim, D. H. Hong, N. G. Yang, Dr. Y. W. Han, Prof. D. K. Moon
Nano and Information Materials (NIMs) Laboratory
Department of Chemical Engineering
Konkuk University
120, Neungdong-ro, Gwangjin-gu, Seoul 05029, Korea
E-mail: dkmoon@konkuk.ac.kr

Dr. S. J. Jeon
Department of Academy of Applied Science and Technology
Konkuk University
120, Neungdong-ro, Gwangjin-gu, Seoul 05029, Korea

The ORCID identification number(s) for the author(s) of this article can be found under https://doi.org/10.1002/solr.202000608.

1. Introduction

Nonfullerene organic solar cells (NFOSCs) offer various benefits, including cost-effectiveness, solution processability, low weight, flexibility, and semi-transparency; in addition, they are ideal for large-scale roll-to-roll processing.[1–6] Recently, NFOSCs have achieved very high power conversion efficiencies (PCEs) of over 17%, both in single solar cells[7–9] and tandem solar cells,[10] and their PCEs are expected to exceed the 20% theoretical limit with further design improvements and the development of superior active materials.[11] Although the PCEs of state-of-the-art NFOSCs have rapidly improved, most of these devices are fabricated using halogenated solvents in an inert atmosphere, which is not amenable to commercialization. In particular, compared with the record efficiencies reported for glove box (GB)-processed organic solar cells (OSCs), the performances of devices produced in air environment (Air) are comparatively very low.[12–16] This reduction in performance is mainly attributed to the air-sensitivity of the donor materials.

Two-dimensional (2D) benzo[1,2-*b*:4,5-*b*′]dithiophene (2DBDT)-based building blocks have been used as donor units in recent years for developing high-performance wide-bandgap polymer donor materials.[8,10,17–19] Their excellent photovoltaic properties and chemical stability, along with easy processability and low cost, make 2DBDT-based polymers promising candidates for use in mass-producible OSCs.[20,21] However, most acceptor units in donor–acceptor polymers still have high synthetic complexity, with numerous synthetic and purification steps, among other issues such as high cost of raw materials.[8,13,16–19,22–24] To address these issues, many researchers have proposed a simple design strategy with carboxylate-functionalized heterocyclic rings as the acceptor unit.[25–31]

The molecular structures of some recently developed carboxylate-functionalized polymer donors are shown in **Figure 1**. Choi and co-workers reported the first example of a
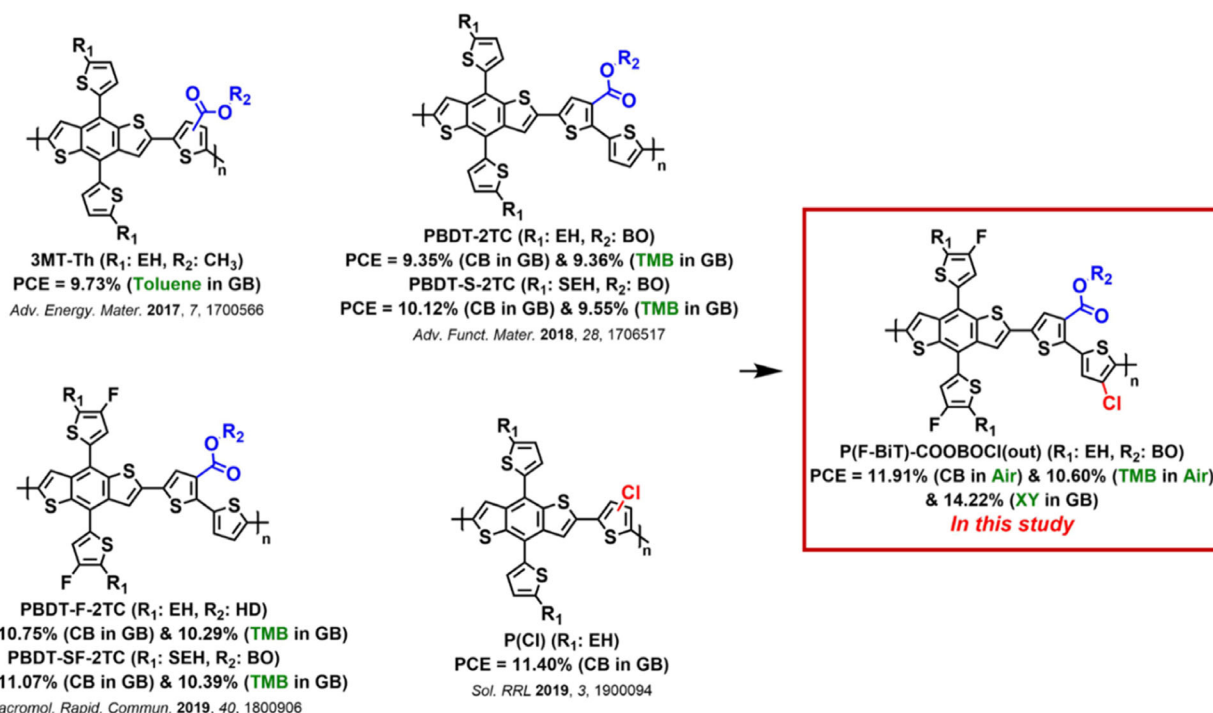
Figure 1. Molecular structures of carboxylate- or chlorine-functionalized polymer donors and the new polymer, P(F-BiT)-COOBOCl(out), developed in this study. EH: 2-ethylhexyl, BO: 2-butyloctyl, HD: 2-hexyldecyl, and XY: o-xylene; GB and Air refer to devices fabricated in GB and air environments, respectively.

methyl carboxylate thiophene-2DBDT-based polymer (3MT-Th; Figure 1a) in 2017.[25] It exhibited a deep-lying highest occupied molecular orbital (HOMO) level of −5.42 eV and good solubility in nonhalogenated solvents. When blended with 3,9-bis(2-methylene-(3-(1,1-dicyanomethylene)-indanone))-5,5,11,11-tetrakis(4-hexylphenyl)-dithieno[2,3-d:2′,3′-d′]-s-indaceno[1,2-b:5,6-b′] dithiophene (ITIC) and processed in toluene, the resultant OSC achieved a high PCE of 9.73% with a high open-circuit voltage (V_{oc}) of 0.95 V, and also excellent shelf-life stability over 1000 h. In 2018, Chen and co-workers reported two high-performance polymers (PBDT-2TC and PBDT-S-2TC; Figure 1b) based on asymmetric bithiophene with one carboxylate group, formed by a facile synthetic approach without halogenated solvents.[26] Among these, PBDT-S-2TC blended with ITIC reached a high PCE of 10.12% when processed in chlorobenzene (CB) and 9.55% PCE using 1,2,4-trimethylbenzene (TMB). In 2019, Chen and co-workers reported enhanced asymmetric polymers (PBDT-F-2TC and PBDT-SF-2TC; Figure 1c) by introducing fluorine and sulfur atoms on the 2DBDT unit, which efficiently lowered the HOMO level and increased the molar coefficient.[27] Optimized devices based on PBDT-SF-2TC blended with 3,9-bis(2-methylene-((3-(1,1-dicyanomethylene)-6,7-difluoro)-indanone))-5,5,11,11-tetrakis(4-hexylphenyl)-dithieno[2,3-d:2′,3′-d′]-s-indaceno[1,2-b:5,6-b′]dithiophene (IT-4F) showed PCEs of 11.07% and 10.29% when processed in CB and TMB, respectively. In the same year, our group reported a low-cost wide-bandgap donor polymer (P(Cl); Figure 1d) based on chlorine-substituted thiophene, which was synthesized in only one step.[32] A blend of P(Cl) with 3,9-bis(2-methylene-(3-(1,1-

dicyanomethylene)11,11-tetrakis(4-hexylthienyl)-thiethieno[2,3-d:2′,3′-d′]-s-indaceno[1,2-b:4,5-b′]dithiophene (ITIC-Th) exhibited high performance with a PCE of 11.4%, of which 91% was maintained after 2000 h of storage. However, despite the good performance and low synthetic complexity of P(Cl), it is hard to efficiently modify it without extending the conjugated length or engineering the side chains, as increasing the molecular weight decreases the solubility. Consequently, this approach presents a trade-off between performance and cost. In addition, chlorine thiophene-based polymers are not soluble in eco-friendly solvents such as toluene, o-xylene (XY), and TMB.[32-34]

In this study, two new 2DBDT-based donor polymers, P(F-BiT)-COOBOCl(in) and P(F-BiT)-COOBOCl(out) (Figure 1e), were designed and synthesized with relatively low synthetic complexity by simultaneous functionalization of the bithiophene unit with chlorine and carboxylate groups. "In" and "out" refer to the inward- and outward-facing direction of the Cl group on the bithiophene unit, respectively. In P(F-BiT)-COOBOCl(out), the synergistic effects of chlorine and carboxylate functionalization showed many advantages, including small dihedral angles between adjacent units, a strong dipole moment, deep-lying HOMO level, and superior air stability. Due to these advantages, the optimized device with IT-4F achieved a PCE of 11.8% with a V_{oc} of 0.899 V; the air-processed device showed the highest PCE of 11.9% with a surprisingly high fill factor (FF) of ≈70%. The high air-processability of the P(F-BiT)-COOBOCl(out):IT-4F cell reflects its potential as an active material for roll-to-roll processing (which inevitably exposes the device to moisture and oxygen). Moreover, when processed using the eco-friendly solvent TMB in air, the

device yielded a relatively high PCE of 10.60% (certified PCE: 10.47% from the Nano Convergence Practical Application Center (NCPAC) in Korea), which is the maximum reported value for NFOSCs fabricated using an eco-friendly solvent in an air environment so far.[12-16] The corresponding P(F-BiT)-COOBOCl(out)-based OCSs, without encapsulation, showed excellent stability during long-term storage (for 1000 h) and light-exposure tests (for 100 h).[5,14,16,23,25,32,34-38]

To further demonstrate the applicability of this eco-friendly process, high-performance devices were fabricated using a blend of P(F-BiT)-COOBOCl(out) and a near-infrared (NIR) acceptor unit, 2,2′-((2Z,2′Z)-((12,13-bis(2-butyloctyl)-3,9-diundecyl-12,13-dihydro-[1,2,5]thiadiazolo[3,4-e]thieno[2″,3″:4′,5′]thieno[2′,3′:4,5]pyrrolo[3,2-g]thieno[2′,3′:4,5]thieno[3,2-b]indole-2,10-diyl)bis(methanylylidene))bis(5,6-dichloro-3-oxo-2,3-dihydro-1H-indene-2,1-diylidene))dimalononitrile (Y6-BO-4Cl). The P(F-BiT)-COOBOCl(out):Y6-BO-4Cl blended device with a conventional structure reached a high PCE of 14.22% when processed using XY. The results demonstrate that the functionalization of bithiophene with both chlorine and carboxylate groups is a promising strategy for producing weak electron-accepting building blocks for wide-bandgap polymers with great potential for use in high-performance NFOSCs, which is expected to benefit the commercialization of OSC devices.

2. Results and Discussion

2.1. Material Design and Synthesis, Physical and Thermal Properties, and Theoretical Calculations

The synthetic routes for producing chlorine- and carboxylate-functionalized bithiophene monomers and their donor polymers are summarized in **Scheme 1**, and the details are described in Figure S1–S6, Supporting Information. As shown in Scheme S1 and S2, Supporting Information, the newly designed routes for each target compound have relatively low synthetic complexity compared with other possible synthetic routes.[27,39,40] As a result, the two brominated monomers BiT-COOBOCl(in) and BiT-COOBOCl(out) were successfully obtained with high overall yields (60.4% and 65.4%, respectively) via straightforward four-step processes. The polymers were prepared via a typical Stille coupling reaction between the brominated monomers and F-2DBDT, and then purified by successive Soxhlet extraction. The polymer structures were confirmed by NMR (Figure S7 and S8, Supporting Information).

Both P(F-BiT)-COOBOCl(in) and P(F-BiT)-COOBOCl(out) exhibited good solubility in common organic solvents including chloroform, toluene, XY, CB, and TMB. The molecular weights of the polymers were determined by gel permeation chromatography (GPC). Comparable number-average molecular weights (M_n) of 14.5 and 52.2 kDa with polydispersity indices (PDI) of 1.67 and 1.78 were obtained for P(F-BiT)-COOBOCl(in) and P(F-BiT)-COOBOCl(out), respectively. The results of thermogravimetric analyses (TGA) confirmed that the decomposition temperature (T_d; temperature at which 5% sample weight loss occurred) for each polymer was above 300 °C (Figure S9, Supporting Information). In addition, differential scanning calorimetry (DSC) measurements revealed that

P(F-BiT)-COOBOCl(in) had a high melting temperature (T_m) of 252 °C, whereas P(F-BiT)-COOBOCl(out) showed no clear thermal transitions, except a glass transition between 30 and 300 °C (Figure S10, Supporting Information).[41,42] Details of the thermal and physical properties of the donor polymers are summarized in **Table 1**.

To better understand the structure–property relationships, density functional theory (DFT) calculations were performed using Gaussian 09 for carboxylate-substituted (BiT-COOMe) and carboxylate-/chlorine-substituted (BiT-COOMeCl(in) and BiT-COOMeCl(out)) bithiophene moieties (Figure S11, Supporting Information). For these calculations, the side chains were substituted with methyl (Me) groups to shorten the computation time. Details of the DFT calculation results are summarized in Table S1, Supporting Information. As shown in Figure S11, Supporting Information, both BiT-COOMe and BiT-COOMeCl(out) exhibited planar structures with small dihedral angles of approximately 20°, whereas BiT-COOMeCl(in) had a large torsion angle of over 70° due to steric hindrance between the carboxylate and chlorine functional groups. This large torsion angle may reduce the probability of reactions during polymerization, resulting in the lower molecular weight of P(F-BiT)-COOBOCl(in).[43,44] The dipole moments and HOMO levels improved with the introduction of chlorine (1.69 D and −6.24 eV for BiT-COOMeCl(in) and 3.22 D and −5.90 eV for BiT-COOMeCl(out) vs 1.37 D and −5.67 eV for BiT-COOMe). As a result, we can expect the chlorine- and carboxylate-substituted moieties to have a stronger charge separation and lower HOMO level relative to that of reported polymers.[27]

To more precisely predict the polymer backbone geometries, electronic structures, and frontier molecular energy levels, theoretical calculations were performed using DFT for polymers with 2 repeating units ($n = 2$), again substituting the side groups with methyl groups to simplify the calculations. As shown in **Figure 2**, the optimized geometries of the P(F-BiT)-COOBOCl(in) and P(F-BiT)-COOBOCl(out) dimers exhibited very different curvatures. The respective dihedral angles (θ_1, θ_2, θ_3, θ_4, and θ_5) between the adjacent carboxylated thiophene, chlorinated thiophene, and F-2DBDT motifs for the $n = 2$ polymers were 10.7°, 65.2°, 15.3°, 10.7°, and 67.5° for P(F-BiT)-COOBOCl(in) and 11.5°, 14.5°, 19.9°, 9.4°, and 19.1° for P(F-BiT)-COOBOCl(out). Thus, P(F-BiT)-COOBOCl(out) likely exhibits greater planarity. This suggests that the chlorine substitution position in the polymer backbone can significantly influence the molecular packing order.

The molecular electrostatic potential (ESP) distribution and dipole moments are also directly related to the chlorine and carboxylate groups. Both polymers show negative ESP values across most of the conjugated backbone, especially around the carboxylate and chlorine groups, which have strong electronegativity. This is expected to increase the intermolecular interaction with IT-4F, which has a relatively positive surface.[45,46] However, for P(F-BiT)-COOBOCl(in), the partially strong negative surfaces are shielded on the conjugated backbone due to the large tilting between adjacent units, which may interrupt the charge transfer with IT-4F. The net dipole moment of P(F-BiT)-COOBOCl(out) was higher than that of P(F-BiT)-COOBOCl(in) (6.67 vs 2.86 D), which is expected to improve the charge separation of the former device.[43]

(a)

(b)
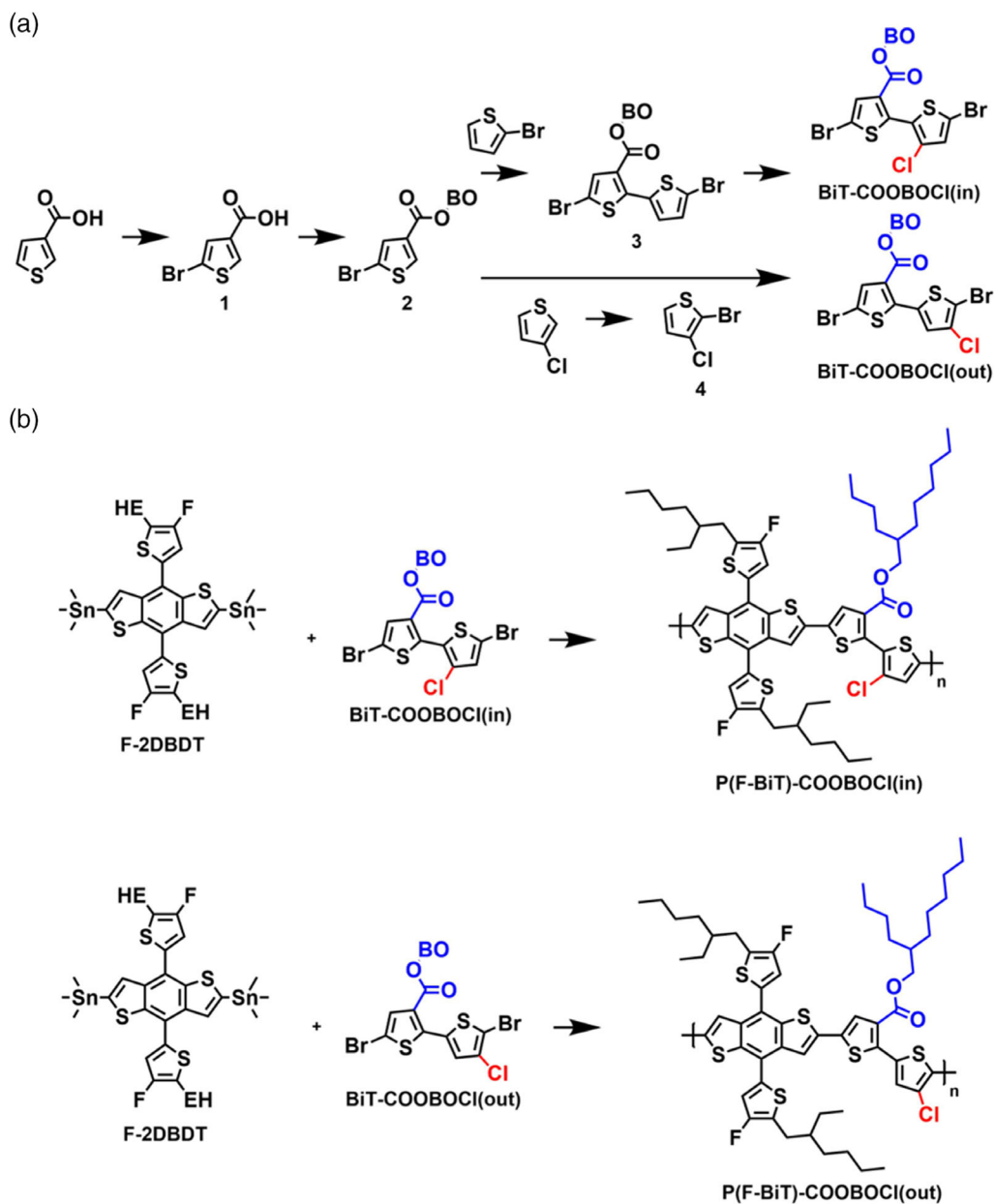
Scheme 1. Synthetic routes to chlorine- and carboxylate-functionalized a) bithiophene monomers and b) donor polymers.

Table 1. Physical and thermal properties of donor polymers.

Polymer	Yield [%]	M_n [kDa][a]	M_w [kDa][a]	PDI[a]	T_d [°C][b]
P(F-BiT)-COOBOCl(in)	74.0	14.5	24.2	1.67	348
P(F-BiT)-COOBOCl(out)	89.0	52.2	93.0	1.78	361

[a]Parameters (M_n: number-average molecular weight; M_w: weight-average molecular weight; PDI: polydispersity index) determined by GPC in chloroform using polystyrene standards; [b]Temperature corresponding to 5% weight loss.

The HOMO and lowest unoccupied molecular orbital (LUMO) energy levels and bandgaps were also estimated for each model compound, as shown in Figure S12, Supporting Information. The results and trends are similar to those of previous calculations for bithiophene moieties.

2.2. Optical and Electrochemical Properties

The optical and electrochemical properties of the polymers were investigated through UV–vis spectroscopy and cyclic voltammetry (CV). The results are summarized in **Table 2**. Both polymers exhibited absorption bands at around 350 nm and 400–600 nm, corresponding to the π–π* transition and intramolecular charge transfer (ICT), respectively; these are complementary with IT-4F, which has a strong absorption band in range of
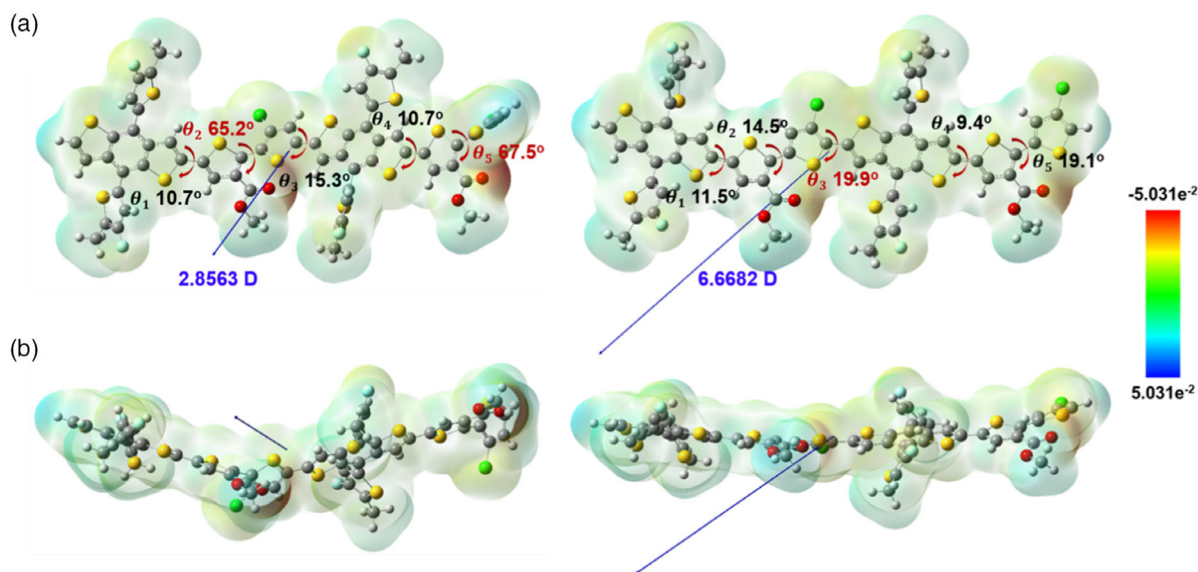
Figure 2. Calculated ESP surfaces of the polymers at $n = 2$: a) top views with dihedral angles (θ_1, θ_2, θ_3, θ_4, and θ_5) and dipole moment and b) their side views (Yellow: sulfur, Green: chlorine, Red: oxygen, Sky blue: fluorine, White: hydrogen, and Gray: carbon).

Table 2. Optical and electrochemical properties of donor polymers.

Polymer	Solution λ_{max} [nm]	Molar coefficient ε [M^{-1} cm^{-1}] at λ_{max} [nm]	Film λ_{max} [nm]	E_g^{opt} [eV][a]	E_{ox}^{onset} [V]	E_{HOMO} [eV][b]	E_{LUMO} [eV][c]
P(F-BiT)-COOBOCl(in)	349, 449	12 908 (349), 18 176 (449)	461	2.15	1.48	−5.71	−3.56
P(F-BiT)-COOBOCl(out)	347, 541	37 206 (347), 82 496 (541)	370, 549, 581	1.92	1.43	−5.66	−3.74

[a]Calculated from the intersection of the tangent on the low energetic edge of the absorption spectrum with the baseline; [b]$E_{HOMO} = -4.8 - [E_{ox}^{onset}$ (vs Ag/AgCl) $- E_{1/2}(Fc/Fc^+$ vs Ag/AgCl)] ($E_{1/2}(Fc/Fc^+$ vs Ag/AgCl) = 0.57 eV); [c]$E_{LUMO} = E_g^{opt} - E_{HOMO}$.

600–800 nm.[18,19,27,29-31,33,34] As shown in **Figure 3**a, the molar absorption coefficients (ε) were calculated using the Beer–Lambert equation[23,32-34] from the UV–vis data recorded in chloroform solutions with different concentrations on the order of 10^{-5} M. The maximum ε values were 1.82×10^4 and 8.25×10^4 M^{-1} cm^{-1} for P(F-BiT)-COOBOCl(in) and P(F-BiT)-COOBOCl(out), respectively. The extinction coefficient of P(F-BiT)-COOBOCl(out) is higher than that reported for many efficient wide-bandgap polymers.[5,23,29-31,34,47] P(F-BiT)-COOBOCl(in) exhibits a relatively low ε because of its low molecular weight and small dipole moment.

Based on their absorption onsets in the film state, P(F-BiT)-COOBOCl(in) and P(F-BiT)-COOBOCl(out) showed wide optical bandgaps (E_g^{opt}) of 2.15 and 1.92 eV, respectively (see Figure 3b). The solution and film states of P(F-BiT)-COOBOCl(in) exhibited drastic differences in the ICT wavelength region due to the high steric hindrance between intramolecular units.[43,44] However, P(F-BiT)-COOBOCl(out) exhibited a broader absorption spectra with a 40 nm red-shifted shoulder peak in the film state. This red-shift is indicative of strong π–π stacking, which leads to enhanced absorption properties.

Next, the frontier molecular energy levels of the polymers were determined from CV measurements. As shown in Figure 3c, P(F-BiT)-COOBOCl(in) exhibited an unstable oxidation peak and negligible reduction peak, whereas P(F-BiT)-COOBOCl(out)

had distinct oxidation and reduction peaks.[5,23,29-31,34,47] The measured HOMO energy levels (E_{HOMO}) of both polymers were determined from the onset oxidation potential (E_{ox}^{onset}) and $E_g^{opt} - E_{HOMO}$, respectively, and by using the following electrochemical equation: $E_{HOMO} = -4.8 - (E_{ox}^{onset} - E_{1/2,ferrocene})$, where $E_{1/2,ferrocene}$ equals 0.57 eV (measured data). The HOMO energy levels of P(F-BiT)-COOBOCl(in) and P(F-BiT)-COOBOCl(out) ($E_{HOMO} = -5.71$ and −5.66 eV, respectively) were in good agreement with the DFT calculation results.

As shown in Figure 3d, it was expected that when the polymers are blended with IT-4F, and the energy levels are well-aligned, the V_{oc} of P(F-BiT)-COOBOCl(in) would be higher than that of P(F-BiT)-COOBOCl(out). However, there is no energy offset between the HOMO levels of P(F-BiT)-COOBOCl(in) and IT-4F, so if the driving force is insufficient, there may be a high probability of charge recombination.[34,48] In contrast, the HOMO level of P(F-BiT)-COOBOCl(out) is slightly higher (by 0.05 eV) than that of IT-4F, which is favorable for photovoltaic performance.

2.3. Photovoltaic Performance

To get the best performance from each polymer, all devices were fabricated and optimized with IT-4F and an inverted device
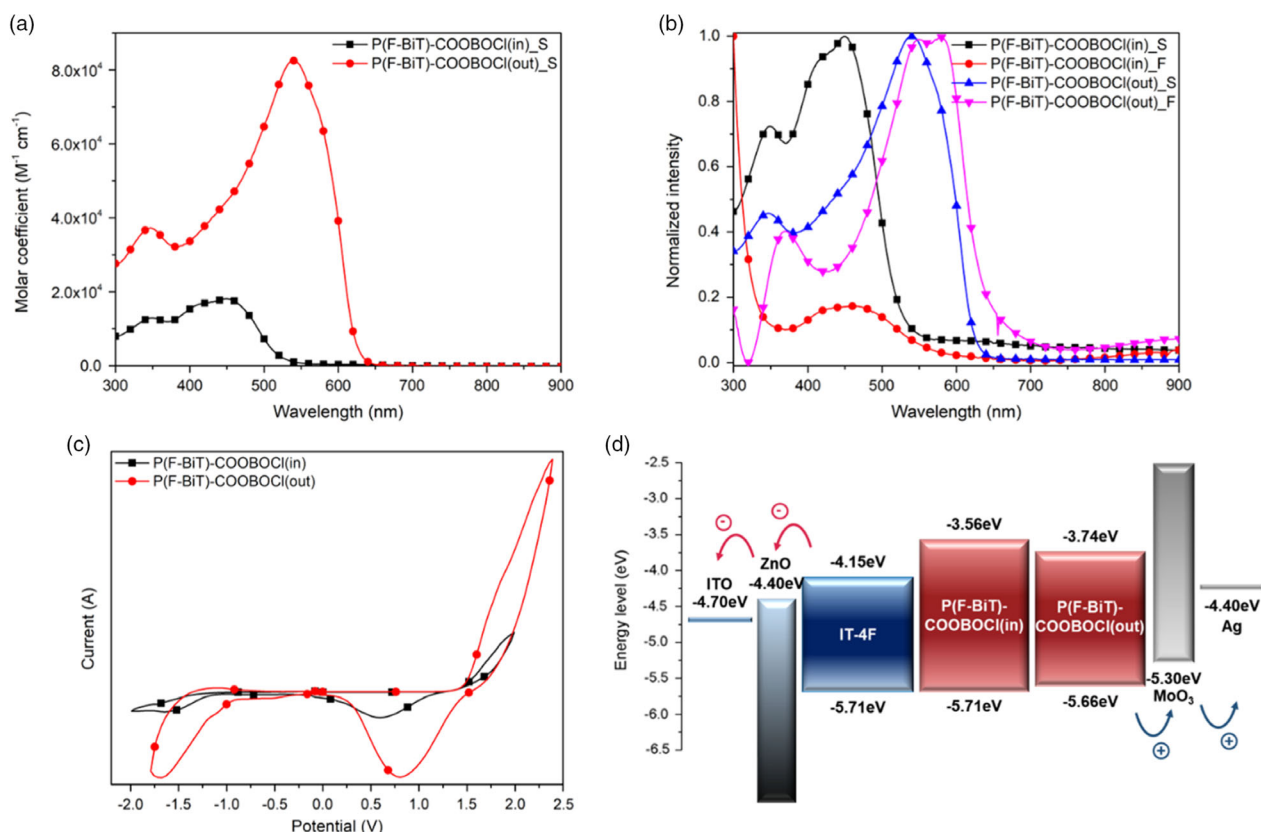
Figure 3. UV–vis absorption spectra, CV curves, and energy band diagrams of the polymers: a) average molar absorption coefficients in chloroform (measured using 10^{-5} M chloroform solutions); b) UV–vis absorption spectra of chloroform solutions (S) and thin films (F); c) CV curves of thin films; and d) energy band diagrams with IT-4F in an inverted structure.

structure (ITO/ZnO/polymer:IT-4F/MoO$_3$/Ag). This improves the device stability compared with conventional devices that use a high work-function metal anode.[49] To optimize each active layer, polymer:IT-4F (1:1, w/w) blended solutions were dissolved in CB or TMB, with 0.5 vol% of 1,8-diiodooctane (DIO) additive, then spin-coated onto the ZnO-coated ITO glass in an air or N$_2$ atmosphere, followed by annealing. The thickness of the polymer:IT-4F layer was controlled to ≈90 nm by tuning the spinning rate during the spin-coating process. The photovoltaic parameters for the optimized polymer blends are summarized in **Table 3**, and detailed information for the P(F-BiT)-COOBOCl(out)-based devices is given in the

Supporting Information; specifically, the current density–voltage (J–V) curves and their parameters for inverted OSCs with respect to the amount of DIO additive (Figure S13 and Table S2, Supporting Information) and post-annealing temperature (Figure S14 and Table S3, Supporting Information).

As shown in **Figure 4**a, the CB-processed device with P(F-BiT)-COOBOCl(in):IT-4F exhibited a very low PCE of 1.0% due to the extremely low short-circuit current density (J_{sc}) and FF value. In contrast, the CB-processed device containing P(F-BiT)-COOBOCl(out):IT-4F showed a remarkably high PCE of 11.8% with a V_{oc} of 0.899 V, J_{sc} of 19.1 mA cm^{-2}, and FF of 68.9%. This high efficiency may result from the optimal HOMO offset

Table 3. Photovoltaic performance of optimized polymer blends for inverted OSCs with respect to process.

Active layer[a]	Conditions[b]	V_{oc} [V]	J_{sc} [mA cm^{-2}]	FF [%]	PCE$_{max}$/PCE$_{ave}$ [%][c]
P(F-BiT)-COOBOCl(in):IT-4F (1:1, w/w)	CB in GB	0.963	2.0	49.8	1.0/0.9 ± 0.06
P(F-BiT)-COOBOCl(out):IT-4F (1:1, w/w)	CB in GB	0.899	19.1	68.9	11.8/11.6 ± 0.23
P(F-BiT)-COOBOCl(out):IT-4F (1:1, w/w)	CB in Air	0.899	18.9	70.3	11.9/11.6 ± 0.31
P(F-BiT)-COOBOCl(out):IT-4F (1:1, w/w)	TMB in Air	0.879	19.9	60.7	10.6/10.4 ± 0.21
P(F-BiT)-COOBOCl(out):IT-4F (1:1, w/w)	TMB in Air[d]	0.859	19.919	61.187	10.467

[a]Post-annealing at 140 °C for 10 min; [b]Solutions contain 0.5% DIO additive; [c]Average PCE values calculated from 10 independent cells; [d]Certification result from the NCPAC, Republic of Korea (No. TP-20S-0758).
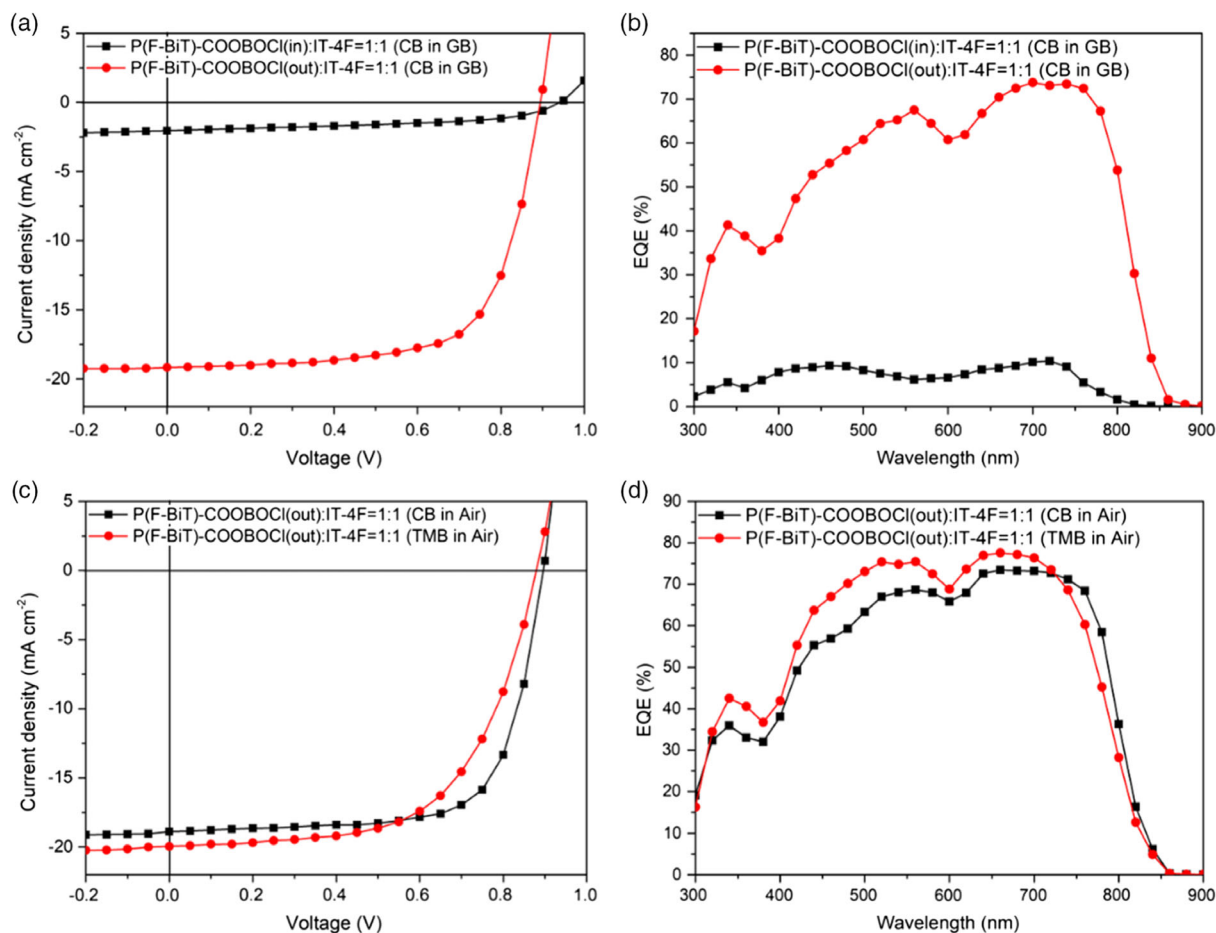
Figure 4. a,c) *J–V* and b,d) EQE curves of the optimized devices for the polymer blends processed with different conditions: a,b) GB and c,d) air environments.

difference between the donor and acceptor units, and from the minimized energy loss (E_{loss}), increasing the probability of charge carrier separation.[50-53] E_{loss} is an important parameter in the evaluation of photovoltaic performance. It can be estimated by the equation $E_{loss} = E_g^{opt} - eV_{oc}$, where E_g^{opt} is the smallest optical bandgap of the donor and acceptor. Considering that E_g^{opt} is 1.56 eV for IT-4F with onset absorption 794 nm and eV_{oc} is 0.899 eV in the P(F-BiT)-COOBOCl(out):IT-4F blend, E_{loss} is calculated as 0.66 eV. E_{loss} values reported in the literature typically range from 0.7 to 1.0 eV;[6,51-53] thus, the E_{loss} of 0.66 V is smaller than that of most OSCs.[3,6]

External quantum efficiency (EQE) curves of the CB-processed devices containing P(F-BiT)-COOBOCl(in):IT-4F and P(F-BiT)-COOBOCl(out):IT-4F are shown in Figure 4b. The EQE of the P(F-BiT)-COOBOCl(in):IT-4F device was very low over the entire wavelength range, similarly to the *J–V* results. In contrast, the P(F-BiT)-COOBOCl(out):IT-4F device displayed a broad EQE response from 300 to 850 nm, and the EQE in the absorption range from 550 to 850 nm reached ≈70%, indicating that both donor and acceptor units contributed greatly to light harvesting. Interestingly, the E_{loss} calculated from the EQE curve for P(F-BiT)-COOBOCl(out):IT-4F device is 0.56 eV, due to the smaller E_g^{opt} of 1.46 eV with onset absorption at 850 nm; thus,

it achieved a smaller E_{loss} relative to the empirical threshold of 0.60 eV.[6,51-53] Such a small E_{loss} is critical for achieving high PCEs in P(F-BiT)-COOBOCl(out)-based NFOSCs.[54]

To evaluate the large-scale processability of the P(F-BiT)-COOBOCl(out) donor polymer, we fabricated a device by spin-coating in air. As shown in Figure 4c,d, the air-processed device containing P(F-BiT)-COOBOCl(out):IT-4F had a slightly higher PCE (11.9%) and FF (70.3%) than the equivalent GB (N₂)-processed device. The EQE curve was very similar to that of the GB-processed device. Reliability tests were conducted on devices processed under different relative humidity (RH) conditions (40%, 50%, 61%, and 69% RH). The devices exhibited an average PCE of 11.7% with excellent stability (Figure S15 and Table S4, Supporting Information).

Moreover, to test the processability in an eco-friendly solvent, a TMB-processed P(F-BiT)-COOBOCl(out):IT-4F device was fabricated in air. This device achieved a high PCE of 10.6% and a J_{sc} of 19.9 mA cm^{-2} (maximized EQE of 77.6% at 660 nm), which, to our knowledge, is among the highest PCEs reported to date for NFOSCs processed with an eco-friendly solvent in air.[5,12-16] To confirm the reliability of the raw state, we sent the cell without any encapsulation to the NCPAC, Republic of Korea and requested a certified measurement. A certified PCE of

10.467% (No. TP-20S-0758) was recorded (Figure S16, Supporting Information). These results demonstrate that the chlorine- and carboxylate-functionalized polymer, P(F-BiT)-COOBOCl(out), is stable against oxygen and moisture in air, due to the deep-lying HOMO level according to the E_{ox}^{onset} of 1.43 eV.[12-16]

2.4. Charge Transport Properties

The charge transfer properties between the donor and acceptor units in the polymer blends must be investigated to clarify their contribution to device performance. Photoluminescence (PL) measurements are a convenient method of probing the charge transfer or energy transfer between materials; thus, PL measurements were performed on films of the pristine polymers and optimized polymer blends.[23,32-34] The results are shown in Figure S17, Supporting Information. Each material exhibited a pronounced PL emission peak in the ranges of 560–900 and 660–900 nm when excited at 500 and 600 nm, respectively; in all the polymer blends, PL quenching (PLQ) was clearly observed in the range of 700–850 nm. The PLQ values and energy-level offsets are summarized in Table S5, Supporting Information.

For the P(F-BiT)-COOBOCl(in):IT-4F blend, the donor to blend (D→B) and acceptor to blend (A→B) PL emissions were partially quenched, with $PLQ_{D→B}$ of 66.8% and $PLQ_{A→B}$ of 47.9% under excitation at 500 nm and $PLQ_{D→B}$ of 66.2% and $PLQ_{A→B}$ of 58.5% under excitation at 600 nm. This partial quenching implies that the photoexcited charge carriers are not transferred well between the constituent parts. This result is consistent with the minimal HOMO offset (0 eV) between P(F-BiT)-COOBOCl(in) and IT-4F in the CV results, which can be caused by charge carrier recombination.[55]

In contrast, there was considerable PLQ between P(F-BiT)-COOBOCl(out) and IT-4F, regardless of the processing conditions, indicating that there was highly efficient exciton dissociation in the bulk heterojunction structure. Notably, the maximized $PLQ_{D→B}$ and $PLQ_{A→B}$ rates for P(F-BiT)-COOBOCl(out):IT-4F (CB in GB) and P(F-BiT)-COOBOCl(out):IT-4F (CB in air) were nearly identical, at 93.0% and 92.4% ($PLQ_{D→B}$) and 91.2% and 90.8% ($PLQ_{A→B}$), respectively, under excitation at 500 nm. The P(F-BiT)-COOBOCl(out):IT-4F (TMB in air) film showed slightly different PLQ behavior to that of (F-BiT)-COOBOCl(out):IT-4F (CB in air), as the former exhibited a lower $PLQ_{A→B}$ rate under excitation at 500 nm. These results are in good agreement with the HOMO offsets and energy loss values, which supports the evaluated photovoltaic parameters for each optimized device.

Next, we measured the space-charge-limited current (SCLC) characteristics of hole-only and electron-only devices to verify the charge transport properties in optimized devices for P(F-BiT)-COOBOCl(in):IT-4F (CB in GB), P(F-BiT)-COOBOCl(out):IT-4F (CB in GB), P(F-BiT)-COOBOCl(out):IT-4F (CB in air), and P(F-BiT)-COOBOCl(out):IT-4F (TMB in air) (Figure S18, Supporting Information).[23,32-34,56] The electron and hole mobilities (μ_e and μ_h, respectively) and their balance (μ_e/μ_h) were calculated using the modified Mott–Gurney equation and summarized in Table S6, Supporting Information. The P(F-BiT)-COOBOCl(in):IT-4F (CB in GB) device showed lower hole and electron mobilities (8.39×10^{-5} and 1.29×10^{-6}, respectively)

and a lower charge transport balance (65.04) than the other devices.[23,28] This may be due to the extremely weak exciton dissociation properties revealed by the PL measurement. For P(F-BiT)-COOBOCl(out):IT-4F, devices prepared using all three sets of conditions (CB in GB, CB in air, TMB in air) showed similar charge transport properties (μ_e: 1.79×10^{-5} to 3.08×10^{-5}, μ_h: 2.77×10^{-5} to 7.05×10^{-5}, and μ_e/μ_h: 3.87–6.46). These results imply that blends of IT-4F and P(F-BiT)-COOBOCl(out) perform well, facilitating charge transport and extraction even when processed in air. This is consistent with the former data.[12-16,57]

2.5. Polymer Blend Morphology

The surface morphologies of the optimized polymer blends of P(F-BiT)-COOBOCl(in):IT-4F (CB in GB), P(F-BiT)-COOBOCl(out):IT-4F (CB in GB), P(F-BiT)-COOBOCl(out):IT-4F (CB in air), and P(F-BiT)-COOBOCl(out):IT-4F (TMB in air) were investigated using atomic force microscopy (AFM) (see **Figure 5**). The blended films were prepared under the same conditions as the optimized devices. The P(F-BiT)-COOBOCl(in):IT-4F (CB in GB) film exhibited bulk phase separation and large domains with a root-mean-square (RMS, R_q) roughness of 0.60 nm and maximum height difference in the z-direction (R_z^{max}) of 7.26 nm. This rough morphology may increase the probability of charge recombination before the charge carriers can reach the donor–acceptor interface, resulting in poor performance.[3,12,23,28,32]

In contrast, all three P(F-BiT)-COOBOCl(out):IT-4F films had relatively smooth and uniform features. The topographies of the P(F-BiT)-COOBOCl(out):IT-4F (CB in GB) and P(F-BiT)-COOBOCl(out):IT-4F (CB in air) films were similar, despite the difference in processing environment, with nanoscale bicontinuous phase separation. These interpenetrating donor–acceptor networks are beneficial for exciton dissociation and charge transport. Although the maximum height difference of the P(F-BiT)-COOBOCl(out):IT-4F (CB in air) film was high ($R_z^{max} = 24.53$ nm), the RMS roughness was lower than that of P(F-BiT)-COOBOCl(out):IT-4F (CB in GB) ($R_q = 2.31$ vs 2.57 nm). The lower RMS roughness should enable defect-free contact with the MoO_3 layer, resulting in increased FF values.[18,58] Furthermore, the P(F-BiT)-COOBOCl(out):IT-4F (TMB in air) film, which is processed with an eco-friendly solvent in air, exhibited fiber-like domains and more distinct phase separation, which is beneficial to high J_{sc}.[27,59] Nevertheless, there were some excessive aggregated defects and larger domains with R_q of 3.60 nm and R_z^{max} of 32.92 nm in the nanoscale network, which may reduce the FF.[9,59] These results correspond well with the PL and SCLC parameters of the photovoltaic devices.

2.6. Nanostructural Analysis

To better understand the nanoscale structures of the pristine polymers and optimized polymer blend films, two-dimensional grazing-incidence X-ray diffraction (2D GIWAXS) measurements were conducted.[5,23-26,29-31,34,47] The results are shown in **Figure 6**. The corresponding line-cut profiles were obtained for all films in the out-of-pane (OOP; along q_{xy}) and in-plane
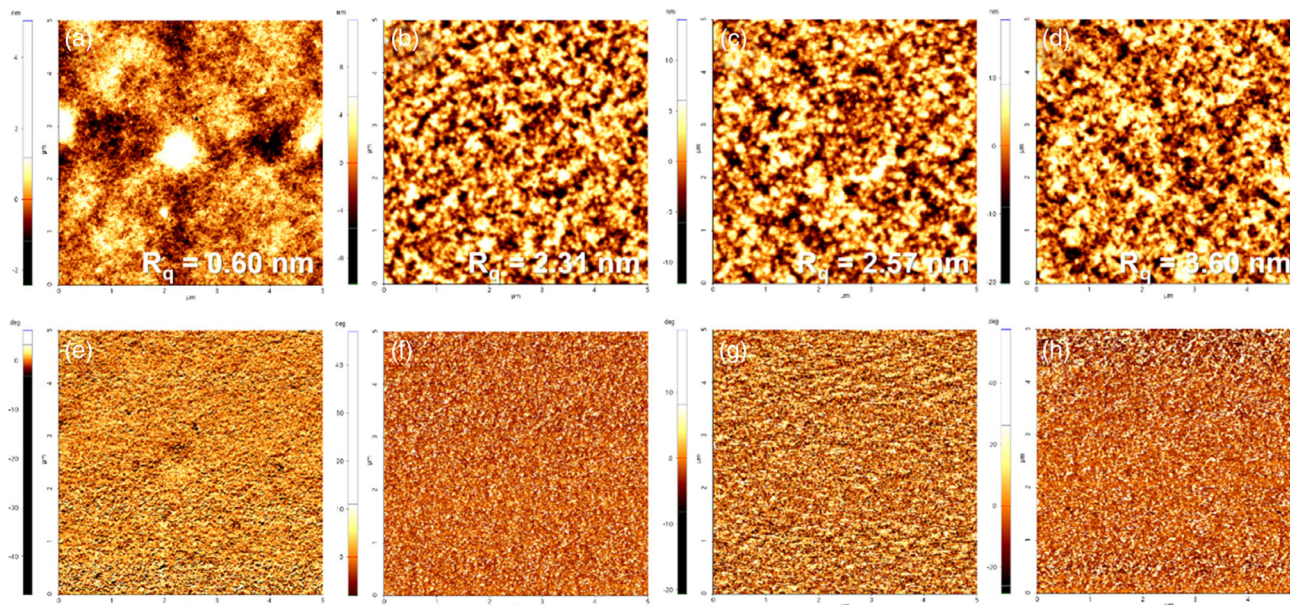
Figure 5. AFM height and phase images (5 µm × 5 µm) for optimized polymer blends processed under different conditions. a,e) P(F-BiT)-COOBOCl(in): IT-4F (CB in GB), b,f) P(F-BiT)-COOBOCl(out):IT-4F (CB in GB), c,g) P(F-BiT)-COOBOCl(out):IT-4F (CB in air), and d,h) P(F-BiT)-COOBOCl(out):IT-4F (TMB in air).

(IP; along q_z) directions (Figure S19a–d, Supporting Information). In addition, intensity-integrated azimuthal pole figure plots were constructed for the (100) scattering peaks of the pristine and blended polymer films (Figure S19e and S19f, Supporting Information). The integrated areas within the azimuthal angle (χ) in the ranges of 0–45° (A_z) and 45–90° (A_{xy}) are defined as the corresponding fractions of face-on and edge-on structures, respectively, and the face-on to edge-on structure ratio, A_{xy}/A_z, was also calculated. Finally, the (100) and (010) crystal coherence lengths ($CCL_{(100)}$ and $CCL_{(010)}$, respectively) in the OOP direction were calculated from the full width at half maximum (FWHM) value using the Scherrer equation. The details of all parameters are summarized in **Table 4** and Table S7, Supporting Information.

For P(F-BiT)-COOBOCl(in) (CB), a single intense (100) peak was observed with a lamellar distance ($d_{(100)}$) of 25.83 Å, indicating the dominant crystalline nature of the polymer, as shown in the profiles of the OOP and IP directions. The P(F-BiT)-COOBOCl(in):IT-4F (CB) blend also exhibited a single (100) peak with $d_{(100)}$ of 25.63 Å. The absence of interchain π–π stacking in P(F-BiT)-COOBOCl(in) (CB) and its blend is attributed to its largely distorted conformational backbone. Upon detailed investigation, P(F-BiT)-COOBOCl(in):IT-4F (CB) was identified to have a A_{xy}/A_z ratio of 0.53 and $CCL_{(100)}$ of 87.455 Å, which confirms that the edge-on structure was more dominant. This result agrees well with the DSC analysis and photovoltaic performance.

In contrast, P(F-BiT)-COOBOCl(out) (CB) exhibited a strong π–π stacking (010) diffraction peak in the OOP direction with a π–π stacking distance ($d_{(010)}$) of 3.86 Å, A_{xy}/A_z ratio of 1.49, and $CCL_{(010)}$ of 24.107 Å, indicating a preferential face-on orientation with tight and pure co-facial packing. The strong π–π stacking suggests that the coplanar polymer backbone of P(F-BiT)-COOBOCl(out) (CB) is favorable for ordered molecular

packing, which will benefit intermolecular charge transport in the vertical direction. This is correlated with the high hole mobility of the polymer.[26,30,33] The (100) and (300) interlamellar distances ($d_{(300)}$) of P(F-BiT)-COOBOCl(out) (CB) were calculated to be 20.11 and 7.23 Å, respectively, with a $CCL_{(100)}$ of 99.295 Å, revealing its high crystallinity. For the P(F-BiT)-COOBOCl(out): IT-4F (CB) blend, an amorphous ring appeared at around 1.4–1.5 Å^{-1} due to the inherent IT-4F stacking properties.[33,60] The P(F-BiT)-COOBOCl(out):IT-4F (CB) blend showed four distinct peaks of (100), (200), (300), and (010), demonstrating both the long-range regularity and high π–π stacking. Furthermore, the P(F-BiT)-COOBOCl(out):IT-4F (CB) blend reached the closest π–π stacking distance (3.61 Å) between (010) planes and balance between the edge-on and face-on structures ($A_{xy}/A_z = 1.00$). The balanced molecular orientation of P(F-BiT)-COOBOCl(out): IT-4F (CB) may be the cause of the high efficiency and reliability of the devices processed in both GB and air.[5,34,57,61,62]

When P(F-BiT)-COOBOCl(out) was processed with an eco-friendly solvent (TMB) in air, the diffraction patterns for the pristine polymer and blended films were similar to those of the CB-processed films, indicating that P(F-BiT)-COOBOCl(out) maintains its inherent stacking properties, regardless of the solvent used for processing. In comparison to P(F-BiT)-COOBOCl(out) (CB), the pristine P(F-BiT)-COOBOCl(out) (TMB) polymer showed enhanced crystallinity, with $d_{(100)}$ of 19.98 Å and $d_{(300)}$ of 7.10 Å, and a closer π–π stacking distance of 3.73 Å. Remarkably, the A_{xy}/A_z ratio of P(F-BiT)-COOBOCl(out) (TMB) was decreased to 0.96, almost without variation of the CCL values. Therefore, it is likely that TMB processing helps to form a high crystalline structure, maintaining crystal quality in both the (100) and (010) directions. However, the P(F-BiT)-COOBOCl(out):IT-4F (TMB) blend exhibited low (100) crystal quality and distant π–π stacking, which
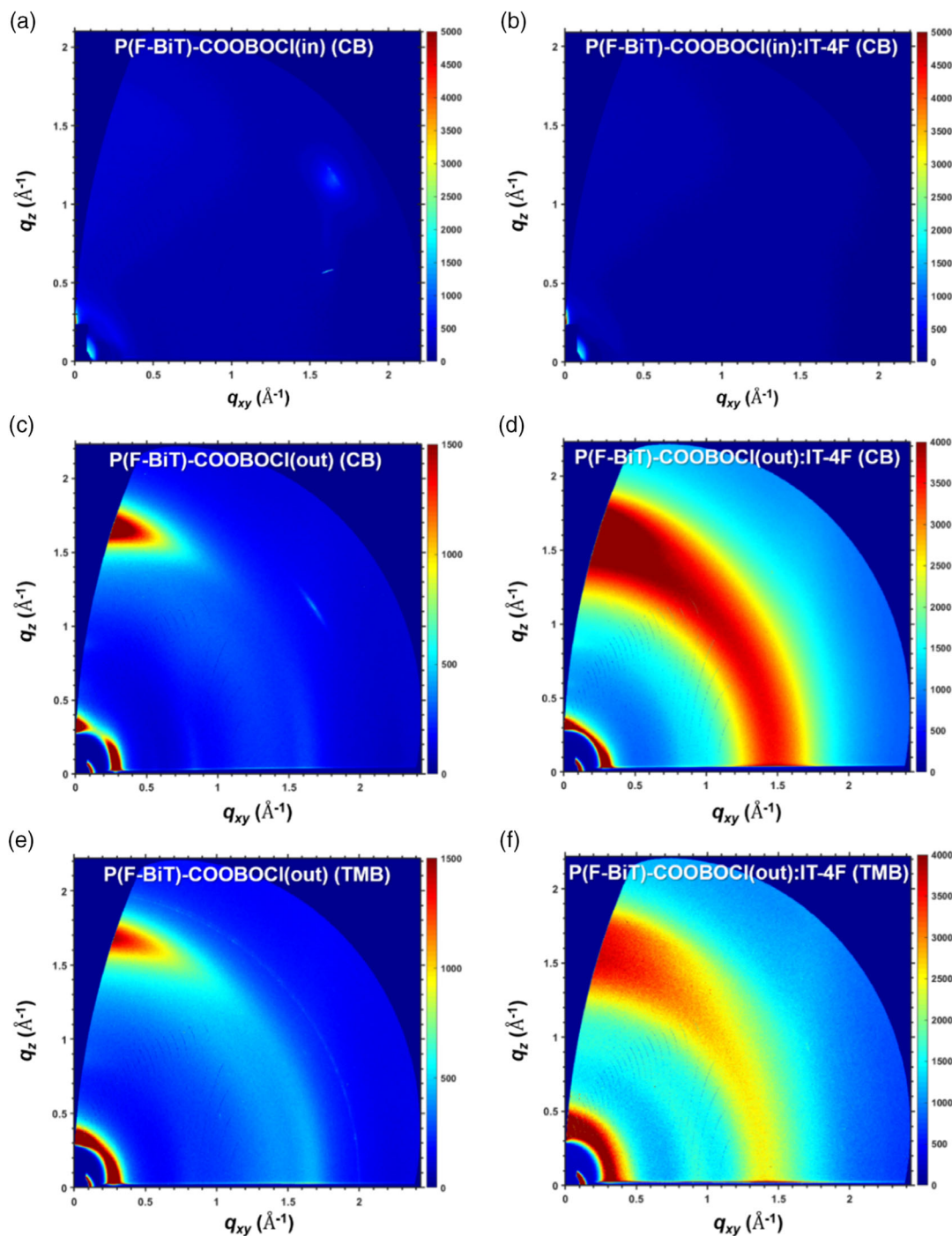
Figure 6. 2D GIWAXS data for films of a,c,e) pristine polymers and b,d,f) their optimized blends processed with different conditions: a) P(F-BiT)-COOBOCl(in) (CB) and b) its blend processed in GB; c) P(F-BiT)-COOBOCl(out) (CB) and d) its blend processed in air; and e) P(F-BiT)-COOBOCl(out) (TMB) and f) its blend processed in air.

prevent charge transport in both the vertical and horizontal directions. This leads to a reduction in photovoltaic performance and FF compared with those of P(F-BiT)-COOBOCl(out):IT-4F (CB).[63] Nevertheless, the eco-friendly solvent and air-processed device successfully reached a PCE of over 10%, with enhanced lamellar packing in both the (100) and (200) directions.

2.7. Storage Lifetime and Photostability

In general, the photoactive organic materials in air-processed OSC devices degrade when exposed to oxygen or moisture, which decreases the device performance over time.[12-16] To evaluate the industrial processability of the air-processed

Table 4. GIWAXS results for the pristine polymers and blend films in the out-of-plane (OOP) direction.

Polymer/polymer blend	Solvent[a]	$d_{(100)}$ [Å] at (100) [Å^{-1}][b]	$d_{(200)}$ [Å] at (200) [Å^{-1}][b]	$d_{(300)}$ [Å] at (300) [Å^{-1}][b]	$d_{(010)}$ [Å] at (010) [Å^{-1}][b]	A_{xy}/A_z[c]
P(F-BiT)-COOBOCl(in) (CB)	CB	25.83 at 0.243	–	–	–	0.88
P(F-BiT)-COOBOCl(out) (CB)	CB	20.11 at 0.312	–	7.23 at 0.869	3.86 at 1.629	1.49
P(F-BiT)-COOBOCl(out) (TMB)	TMB	19.98 at 0.314	–	7.10 at 0.885	3.73 at 1.685	0.96
P(F-BiT)-COOBOCl(in):IT-4F (1:1, w/w)	CB	25.63 at 0.245	–	–	–	0.53
P(F-BiT)-COOBOCl(out):IT-4F (1:1, w/w)	CB	20.61 at 0.305	10.68 at 0.588	7.13 at 0.881	3.61 at 1.739	1.00
P(F-BiT)-COOBOCl(out):IT-4F (1:1, w/w)	TMB	17.06 at 0.368	10.51 at 0.598	–	4.00 at 1.572	0.92

[a] Solutions contain 0.5% DIO additive; [b] q_{xy} (or q_z) = $2\pi/d_{(010)}$ (or $d_{(h00)}$); [c] Ratio of face-on to edge-on orientation determined by the pole figure analysis, where A_{xy} and A_z correspond to the face-on and edge-on fractions, respectively.

P(F-BiT)-COOBOCl(out):IT-4F (CB) and P(F-BiT)-COOBOCl(out):IT-4F (TMB) devices, the shelf-life and photostability were investigated (without encapsulation). The shelf-life stability was studied by storing the devices at room temperature (RT) of 25 °C in an air environment with a RH of 40–50% for up to 1000 h. These conditions are in line with the International Summit on OSC Stability (ISOS) shelf protocol (ISOS-D-1).[5,14,16,23,25,32,34,35,38] In addition, the photostability tests

were performed according to the ISOS-L-1 protocol under continuous AM 1.5 G illumination at 1 sun at 40–50 °C (without a cooling system) in air with RH 40–50%.[23,25,35-37,64] The results are shown in **Figure 7**.

As shown in Figure 7a, the P(F-BiT)-COOBOCl(out):IT-4F (CB in air) device had an initial PCE of 11.51% with a V_{oc} of 0.879 V, J_{sc} of 18.8 mA cm^{-2}, and FF of 69.8%. After 12 h, the PCE increased to its maximum value of 11.9% without
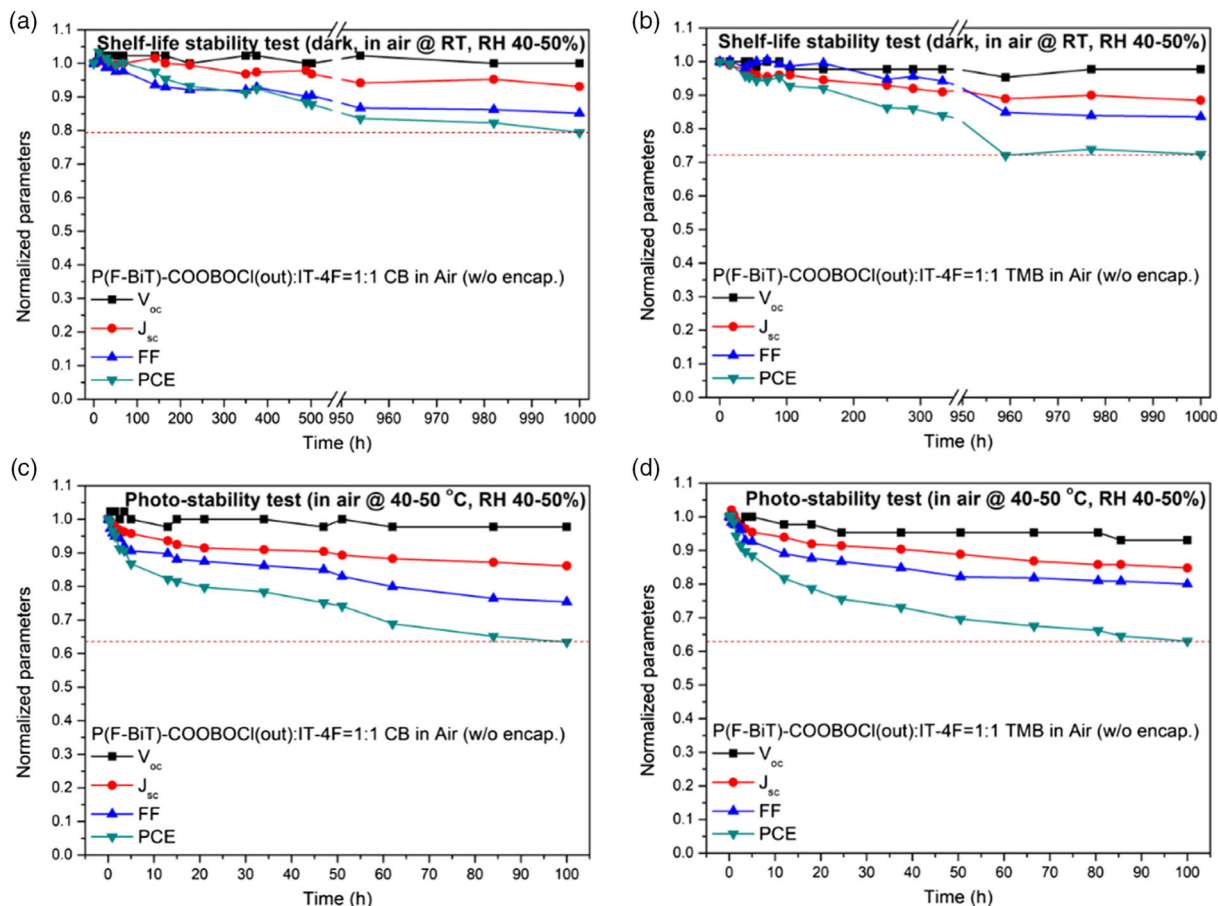

Figure 7. a,b) Storage lifetime (obtained using the ISOS-D-1 shelf protocol; dark, in air, RT, 25 °C, 40–50% RH) and c,d) photostability (obtained using the ISOS-L-1 protocol under continuous AM 1.5G illumination at 1 sun; in air, 40–50 °C, 40–50% RH) for the P(F-BiT)-COOBOCl(out)-based optimized devices without encapsulation: a,c) P(F-BiT)-COOBOCl(out):IT-4F (CB in air) and b,d) P(F-BiT)-COOBOCl(out):IT-4F (TMB in air).

any burn-in loss. The CB-processed device showed excellent air-stability for 1000 h, maintaining approximately 80% of its initial PCE ($PCE_{1000h} = 9.14\%$, with a V_{oc} of 0.879 V, J_{sc} of 17.5 mA cm^{-2}, and FF of 59.4%). Even compared to the GB-processed device, there was only a 10% difference in efficiency up to 1000 h (Figure S20, Supporting Information). We believe the high stability of the air-processed device is primarily due to the balanced face-on to edge-on structure ratio and morphology close to the thermodynamic equilibrium state.[34,65]

Moreover, as shown in Figure 7b, when the P(F-BiT)-COOBOCl(out):IT-4F device was processed with an eco-friendly solvent (TMB) in air, it still maintained 72.3% of its initial PCE up to 1000 h ($PCE_{1000h} = 10.6\%$, with a V_{oc} of 0.879 V, J_{sc} of 19.9 mA cm^{-2}, and FF of 60.7%). This result suggests that the chlorine- and carboxylate-functionalized P(F-BiT)-COOBOCl(out)-based bulk heterojunction is sufficiently stable for long time in air, regardless of the processing solvent.[12,14,16,23,25,32,34,35,38]

The photostability results are shown in Figure 7c,d. The performance of both devices decreased rapidly during the first 5 h of operation, which is associated with burn-in loss due to strong UV damage[36] and spinodal demixing of the donor and acceptor phases.[42] Subsequently, the PCEs remain relatively steady up to 100 h. In short, both devices maintained PCEs of over 63% of their initial values for 100 h, suggesting reasonable photostability of the photoactive materials and NFOSC devices.[23,25,35-37,66,67]

2.8. Potential for High-Performance Devices Fabricated by Eco-Friendly Process with NIR Acceptor

To further demonstrate the applicability of the eco-friendly process, the latest popular NIR nonfullerene acceptor unit, Y6-BO-4Cl (also known as BTP-BO-4Cl), was used to prepare polymer blends instead of IT-4F. Among the Y6 derivatives, Y6-BO-4Cl offers high solubility in solvents with low toxicity, enabling its use in eco-friendly processes.[68,69] The molecular structures and energy levels of P(F-BiT)-COOBOCl(out) and Y6-BO-4Cl are shown in **Figure 8**a. Similar to the P(F-BiT)-COOBOCl(in):IT-4F blend, there is zero HOMO offset between the donor and acceptor units in a P(F-BiT)-COOBOCl(out):

Y6-BO-4Cl blend. Therefore, if the driving force is insufficient, the charge recombination is expected to be high. However, as shown in Figure 8b, Y6-BO-4Cl-based devices with a conventional structure exhibited unexpectedly high PCEs of 12.26% and 14.22% when prepared using halogenated (CB with 0.5% DIO) and nonhalogenated (XY with 0.25% 1-phenylnaphthalene (PN)) solvents, respectively. The high PCEs are probably due to the reasonably enhanced V_{oc} and J_{sc} values derived from the extremely low E_{loss} of approximately 0.44–0.45 eV, which contributes to fast and efficient charge separation, compared with IT-4F-based devices.[70] As shown in Figure 8c, the corresponding EQE curves exhibited suitable responses in the NIR region of 800–950 nm. Moreover, the experimental values show a small deviation with ≈4% mismatch compared with the calculated J_{sc} values.

To better understand the performance of these devices, the molar absorption coefficient profiles of the blended films were investigated with respect to solution combination under optimized device conditions (optimal thickness: 100 nm). The results are shown in Figure S21, Supporting Information. In short, all XY-processed films except for that with 1.0% PN showed higher molar coefficients than the CB-processed films across the entire absorption range, indicating that both the donor and acceptor units contribute greatly to light harvesting in the device. Although the XY (1.0% PN)-processed film showed the largest red-shifted onset value due to the enhanced π–π stacking, the ICT effect was weaker than that in other films with regard to the molar coefficient of the acceptor. The results agree well with the photovoltaic parameters of the fabricated devices, particularly the J_{sc} values.

The detailed photovoltaic performances of the fabricated devices with P(F-BiT)-COOBOCl(out):Y6-BO-4Cl are summarized in Table S8, Supporting Information. Most Y6-derived high-performance wide-bandgap polymers adopt a donor–π–acceptor–π type structure, except for PTQ10 and PTQ11.[71] It probably helped to facilitate the planarity of polymer backbone in the blend and enabling efficiently charge hopping with Y6 derivatives. These valuable results show that P(F-BiT)-COOBOCl(out), as a donor–acceptor or donor–π–π polymer, is highly compatible with Y6 derivatives, and thus can be utilized in the near future in the development of high-performance and eco-friendly NFOSCs.
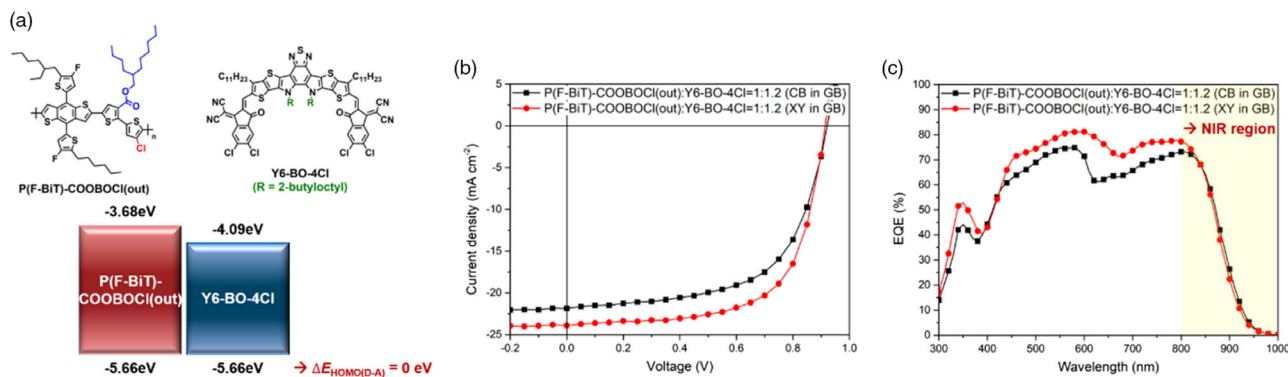

Figure 8. a,b) J–V and c) EQE curves of the optimized devices for the polymer blends processed with different conditions: a,b) GB and c,d) air environments.

3. Conclusion

Herein, two new chlorine- and carboxylate-functionalized bithiophene-based wide-bandgap donor polymers were successfully designed and synthesized. By altering the chlorine and carboxylate substitution topology on the bithiophene moiety, the characterization results were considerably different for P(F-BiT)-COOBOCl(in) and P(F-BiT)-COOBOCl(out). Both polymers exhibited high solubility in eco-friendly solvents despite their low synthetic complexity. In particular, P(F-BiT)-COOBOCl(out), a polymer with outward Cl on bithiophene, had a simultaneously high molecular weight, dipole moment, molar coefficient, planarity, and deep-lying HOMO level. When blended with IT-4F, the resultant air-processed device reached a very high PCE of 11.91%. In addition, the device exhibited superior shelf-life stability and photostability in ambient atmosphere without encapsulation, as well as reduced performance loss relative to most reported NFOSCs. More surprisingly, when prepared with an eco-friendly solvent (TMB) and processed in air, the device reached a high PCE of 10.6% (certified PCE: 10.467%), which is, to our knowledge, among the highest PCEs reported so far for NFOSCs processed under such conditions. Finally, to further demonstrate the potential of this high-performance polymer that can be processed using eco- friendly conditions, we fabricated devices with latest popular NIR acceptor, Y6-BO-4Cl, and achieved the best PCE of 14.22% when using XY solvent. This study gives many perspectives and opportunities for designing and developing efficient photoactive materials as a new strategy for the commercialization of NFOSCs.

4. Experimental Section

Polymerization of poly[(2,6-(4,8-bis(5-(2-ethylhexyl)-4-fluorothiophen-2-yl)-benzo[1,2-*b*:4,5-*b*′]dithiophene))-alt-(2-butyloctyl-5,5′-dibromo-4′-chloro-2,2′-bithiophene-3-carboxylate)] (P(F-BiT)-COOBOCl(out)): A mixture of F-2DBDT (94.05 mg, 0.10 mmol), BiT-COOBOCl(out) (57.1 mg, 0.10 mmol), Pd₂(dba)₃ (3.0 mg), and P(*o*-toly)₃ (10.0 mg) was added to a 10–20 mL vial in an air environment. The vial was capped and evacuated for 20 min before it was refilled with nitrogen gas, after which anhydrous toluene (3.0 mL) was added to the mixture. The reactor was twice degassed and refilled with nitrogen. The polymerization mixture was stirred at 100 °C for 5 h. The polymer was end-capped by the addition of 2-bromothiophene (56.0 mg, 0.33 mmol), and the mixture was further heated at 140 °C for 1 h. After heating, 2-tributylstannyl thiophene (31.3 mg, 0.0875 mmol) was added and the mixture was heated again at 140 °C for 1 h. The reaction mixture was cooled to RT and poured into methanol (300 mL) and 37% HCl (10 mL), stirred for 1 h, and then purified further using a Soxhlet extractor with methanol (24 h), acetone (24 h), hexane (24 h), methylene chloride (24 h), and chloroform (24 h), sequentially. The chloroform fraction of the polymer was reprecipitated in methanol, filtered, and vacuum dried to obtain P(F-BiT)-COOBOCl(out) (dark red solid; yield: 89%). P(F-BiT)-COOBOCl(in) was synthesized under the same conditions with the same procedure (orange to reddish solid; yield: 74.0%).

Supporting Information

Supporting Information is available from the Wiley Online Library or from the author.

Conflict of Interest

The authors declare no conflict of interest.

[1] A. J. Heeger, *Adv. Mater.* **2014**, *26*, 10.
[2] Y. Li, G. Xu, C. Cui, Y. Li, *Adv. Energy Mater.* **2018**, *8*, 1701791.
[3] R. Xue, J. Zhang, Y. Li, Y. Li, *Small* **2018**, *14*, 1801793.
[4] J. Liu, S. Chen, D. Qian, B. Gautam, G. Yang, J. Zhao, J. Bergqvist, F. Zhang, W. Ma, H. Ade, O. Inganäs, K. Gundogdu, F. Gao, H. Yan, *Nat. Energy* **2016**, *1*, 16089.
[5] Y. W. Han, S. J. Jeon, H. S. Lee, H. Park, K. S. Kim, H.-W. Lee, D. K. Moon, *Adv. Energy Mater.* **2019**, *9*, 1902065.
[6] J. Zhang, H. S. Tan, X. Guo, A. Facchetti, H. Yan, *Nat. Energy* **2018**, *3*, 720.
[7] J. Yuan, Y. Zhang, L. Zhou, G. Zhang, H.-L. Yip, T.-K. Lau, X. Lu, C. Zhu, H. Peng, P. A. Johnson, M. Leclerc, Y. Cao, J. Ulanski, Y. Li, Y. Zou, *Joule* **2019**, *3*, 1140.
[8] Q. Liu, Y. Jiang, K. Jin, J. Qin, J. Xu, W. Li, J. Xiong, J. Liu, Z. Xiao, K. Sun, S. Yang, X. Zhang, L. Ding, *Sci. Bull.* **2020**, *65*, 272.
[9] Y. Cui, H. Yao, J. Zhang, K. Xian, T. Zhang, L. Hong, Y. Wang, Y. Xu, K. Ma, C. An, C. He, Z. Wei, F. Gao, J. Hou, *Adv. Mater.* **2020**, *32*, 1908205.
[10] L. Meng, Y. Zhang, X. Wan, C. Li, X. Zhang, Y. Wang, X. Ke, Z. Xiao, L. Ding, R. Xia, H.-L. Yip, Y. Cao, Y. Chen, *Science* **2018**, *361*, 1094.
[11] Y. Firdaus, V. M. Le Corre, J. I. Khan, Z. Kan, F. Laquai, P. M. Beaujuge, T. D. Anthopoulos, *Adv. Sci.* **2019**, *6*, 1802028.
[12] T. Ma, K. Jiang, S. Chen, H. Hu, H. Lin, Z. Li, J. Zhao, Y. Liu, Y.-M. Chang, C.-C. Hsiao, H. Yan, *Adv. Energy Mater.* **2015**, *5*, 1501282.
[13] K. An, W. Zhong, L. Ying, P. Zhu, B. Fan, Z. Li, N. Li, F. Huang, Y. Cao, *J. Mater. Chem. C* **2020**, *8*, 270.
[14] P. Li, M. Mainville, Y. Zhang, M. Leclerc, B. Sun, R. Izquierdo, D. Ma, *Small* **2019**, *15*, 1804671.
[15] N.-W. Teng, C.-H. Li, W.-C. Lo, Y.-S. Tsai, C.-Y. Liao, Y.-W. You, H.-L. Ho, W.-L. Li, C.-C. Lee, W.-C. Lin, Y.-M. Chang, *Sol. RRL* **2020**, *4*, 2000223.
[16] Y. Xu, J. Yuan, S. Zhou, M. Seifrid, L. Ying, B. Li, F. Huang, G. C. Bazan, W. Ma, *Adv. Funct. Mater.* **2019**, *29*, 1806747.
[17] H. Bin, L. Gao, Z.-G. Zhang, Y. Yang, Y. Zhang, C. Zhang, S. Chen, L. Xue, C. Yang, M. Xiao, Y. Li, *Nat. Commun.* **2016**, *7*, 13651.
[18] S. Zhang, Y. Qin, J. Zhu, J. Hou, *Adv. Mater.* **2018**, *30*, 1800868.

[19] B. Fan, X. Du, F. Liu, W. Zhong, L. Ying, R. Xie, X. Tang, K. An, J. Xin, N. Li, W. Ma, C. J. Brabec, F. Huang, Y. Cao, *Nat. Energy* **2018**, *3*, 1051.

[20] M. Jørgensen, K. Norrman, S. A. Gevorgyan, T. Tromholt, B. Andreasen, F. C. Krebs, *Adv. Mater.* **2012**, *24*, 580.

[21] H. Yao, L. Ye, H. Zhang, S. Li, S. Zhang, J. Hou, *Chem. Rev.* **2016**, *116*, 7397.

[22] R. Po, G. Bianchi, C. Carbonera, A. Pellegrino, *Macromolecules* **2015**, *48*, 453.

[23] J. E. Yu, S. J. Jeon, J. Y. Choi, Y. W. Han, E. J. Ko, D. K. Moon, *Small* **2019**, *15*, 1805321.

[24] Y. Tang, H. Sun, Z. Wu, Y. Zhang, G. Zhang, M. Su, X. Zhou, X. Wu, W. Sun, X. Zhang, B. Liu, W. Chen, Q. Liao, H. Y. Woo, X. Guo, *Adv. Sci.* **2019**, *6*, 1901773.

[25] G. E. Park, S. Choi, S. Y. Park, D. H. Lee, M. J. Cho, D. H. Choi, *Adv. Energy Mater.* **2017**, *7*, 1700566.

[26] Y. An, X. Liao, L. Chen, J. Yin, Q. Ai, Q. Xie, B. Huang, F. Liu, A. K.-Y. Jen, Y. Chen, *Adv. Funct. Mater.* **2018**, *28*, 1706517.

[27] S. Huang, W. Gu, L. Chen, Z. Liao, Y. An, C. An, Y. Chen, J. Hou, *Macromol. Rapid Commun.* **2019**, *40*, 1800906.

[28] D. Liu, B. Yang, B. Jang, B. Xu, S. Zhang, C. He, H. Y. Woo, J. Hou, *Energy Environ. Sci.* **2017**, *10*, 546.

[29] S. Li, L. Ye, W. Zhao, H. Yan, B. Yang, D. Liu, W. Li, H. Ade, J. Hou, *J. Am. Chem. Soc.* **2018**, *140*, 7159.

[30] H. Guo, Y. Zhang, L. Chen, X. Liao, Q. Xie, Y. Cui, B. Huang, C. Yang, Y. Chen, *J. Mater. Chem. A* **2019**, *7*, 27394.

[31] D. Liu, Y. Zhang, L. Zhan, T.-K. Lau, H. Yin, P. W. K. Fong, S. K. So, S. Zhang, X. Lu, J. Hou, H. Chen, W.-Y. Wong, G. Li, *J. Mater. Chem. A* **2019**, *7*, 14153.

[32] S. J. Jeon, Y. W. Han, D. K. Moon, *Sol. RRL* **2019**, *3*, 1900094.

[33] S. J. Jeon, Y. W. Han, D. K. Moon, *Small* **2019**, *15*, 1902598.

[34] S. J. Jeon, Y. W. Han, Y. H. Kim, D. K. Moon, *Sol. RRL* **2020**, *4*, 2000074.

[35] D. Baran, R. S. Ashraf, D. A. Hanifi, M. Abdelsamie, N. Gasparini, J. A. Röhr, S. Holliday, A. Wadsworth, S. Lockett, M. Neophytou, C. J. M. Emmott, J. Nelson, C. J. Brabec, A. Amassian, A. Salleo, T. Kirchartz, J. R. Durrant, I. McCulloch, *Nat. Mater.* **2017**, *16*, 363.

[36] J. Lee, J. W. Kim, S. A. Park, S. Y. Son, K. Choi, W. Lee, M. Kim, J. Y. Kim, T. Park, *Adv. Energy Mater.* **2019**, *9*, 1901829.

[37] S. Park, H. J. Son, *J. Mater. Chem. A* **2019**, *7*, 25830.

[38] J. Song, L. Ye, C. Li, J. Xu, S. Chandrabose, K. Weng, Y. Cai, Y. Xie, P. O'Reilly, K. Chen, J. Zhou, Y. Zhou, J. M. Hodgkiss, F. Liu, Y. Sun, *Adv. Sci.* **2020**, *7*, 2001986.

[39] Y. Wu, C. An, L. Shi, L. Yang, Y. Qin, N. Liang, C. He, Z. Wang, J. Hou, *Angew. Chem., Int. Ed.* **2018**, *57*, 12911.

[40] R. Heuvel, F. J. M. Colberts, M. M. Wienk, R. A. J. Janssen, *J. Mater. Chem. C* **2018**, *6*, 3731.

[41] Q. Fan, W. Su, X. Guo, B. Guo, W. Li, Y. Zhang, K. Wang, M. Zhang, Y. Li, *Adv. Energy Mater.* **2016**, *6*, 1600430.

[42] N. Li, J. D. Perea, T. Kassar, M. Richter, T. Heumueller, G. J. Matt, Y. Hou, N. S. Güldal, H. Chen, S. Chen, S. Langner, M. Berlinghof, T. Unruh, C. J. Brabec, *Nat. Commun.* **2017**, *8*, 14521.

[43] S. J. Jeon, Y. W. Han, D. K. Moon, *ACS Appl. Mater. Interfaces* **2019**, *11*, 9239.

[44] S. J. Jeon, J. E. Yu, Y. W. Han, I. S. Suh, D. K. Moon, *J. Ind. Eng. Chem.* **2019**, *71*, 137.

[45] H. Yao, D. Qian, H. Zhang, Y. Qin, B. Xu, Y. Cui, R. Yu, F. Gao, J. Hou, *Chin. J. Chem.* **2018**, *36*, 491.

[46] R. Wang, B. Wang, J. Wang, X. Zhang, D. Zhang, D. Wei, X. Sun, H. Zhou, Y. Zhang, *J. Mater. Chem. A* **2019**, *7*, 25808.

[47] Q. Wang, M. Li, X. Zhang, Y. Qin, J. Wang, J. Zhang, J. Hou, R. A. J. Janssen, Y. Geng, *Macromolecules* **2019**, *52*, 4464.

[48] J. Zhang, W. Liu, G. Zhou, Y. Yi, S. Xu, F. Liu, H. Zhu, X. Zhu, *Adv. Energy Mater.* **2020**, *10*, 1903298.

[49] Z. He, C. Zhong, S. Su, M. Xu, H. Wu, Y. Cao, *Nat. Photonics* **2012**, *6*, 591.

[50] S. Li, L. Zhan, C. Sun, H. Zhu, G. Zhou, W. Yang, M. Shi, C. Z. Li, J. Hou, Y. Li, H. Chen, *J. Am. Chem. Soc.* **2019**, *141*, 3073.

[51] Y. Qin, S. Zhang, Y. Xu, L. Ye, Y. Wu, J. Kong, B. Xu, H. Yao, H. Ade, J. Hou, *Adv. Energy Mater.* **2019**, *9*, 1901823.

[52] X. Zhang, N. Yao, R. Wang, Y. Li, D. Zhang, G. Wu, J. Zhou, X. Li, H. Zhang, J. Zhang, Z. Wei, C. Zhang, H. Zhou, F. Zhang, Y. Zhang, *Nano Energy* **2020**, *75*, 105032.

[53] B. Huang, L. Chen, X. Jin, D. Chen, Y. An, Q. Xie, Y. Tan, H. Lei, Y. Chen, *Adv. Funct. Mater.* **2018**, *28*, 1800606.

[54] Q. Fan, T. Liu, W. Gao, Y. Xiao, J. Wu, W. Su, X. Guo, X. Lu, C. Yang, H. Yan, M. Zhang, Y. Li, *J. Mater. Chem. A* **2019**, *7*, 15404.

[55] V. Lami, Y. J. Hofstetter, J. F. Butscher, Y. Vaynzof, *Adv. Electron. Mater.* **2020**, *6*, 2000213.

[56] R. Peng, Z. Liu, Q. Guan, L. Hong, W. Song, Q. Wei, P. Gao, J. Huang, X. Fan, M. Wang, Z. Ge, *J. Mater. Chem. A* **2018**, *6*, 6327.

[57] L. Yang, S. Zhang, C. He, J. Zhang, Y. Yang, J. Zhu, Y. Cui, W. Zhao, H. Zhang, Y. Zhang, Z. Wei, J. Hou, *Chem. Mater.* **2018**, *30*, 2129.

[58] Y. Huang, E. J. Kramer, A. J. Heeger, G. C. Bazan, *Chem. Rev.* **2014**, *114*, 7006.

[59] L. Ye, Y. Xiong, S. Li, M. Ghasemi, N. Balar, J. Turner, A. Gadisa, J. Hou, B. T. O'Connor, H. Ade, *Adv. Funct. Mater.* **2017**, *27*, 1702016.

[60] M. Chen, D. Liu, W. Li, R. S. Gurney, D. Li, J. Cai, E. L. K. Spooner, R. C. Kilbride, J. D. McGettrick, T. M. Watson, Z. Li, R. A. L. Jones, D. G. Lidzey, T. Wang, *ACS Appl. Mater. Interfaces* **2019**, *11*, 26194.

[61] S. Chen, H. Yao, Z. Li, O. M. Awartani, Y. Liu, Z. Wang, G. Yang, J. Zhang, H. Ade, H. Yan, *Adv. Energy Mater.* **2017**, *7*, 1602304.

[62] L. Zhang, X. Xu, B. Lin, H. Zhao, T. Li, J. Xin, Z. Bi, G. Qiu, S. Guo, K. Zhou, X. Zhan, W. Ma, *Adv. Mater.* **2018**, *30*, 1805041.

[63] Y. Wang, X. Wang, B. Lin, Z. Bi, X. Zhou, H. B. Naveed, K. Zhou, H. Yan, Z. Tang, W. Ma, *Adv. Energy Mater.* **2020**, *10*, 2000826.

[64] P. Liu, S. Dong, F. Liu, X. Hu, L. Liu, Y. Jin, S. Liu, X. Gong, T. P. Russell, F. Huang, Y. Cao, *Adv. Funct. Mater.* **2015**, *25*, 6458.

[65] Z. Liang, M. Li, Q. Wang, Y. Qin, S. J. Stuard, Z. Peng, Y. Deng, H. Ade, L. Ye, Y. Geng, *Joule* **2020**, *4*, 1278.

[66] Z. Jiang, F. Wang, K. Fukuda, A. Karki, W. Huang, K. Yu, T. Yokota, K. Tajima, T.-Q. Nguyen, T. Someya, *Proc. Natl. Acad. Sci. U. S. A.* **2020**, *117*, 6391.

[67] G. P. Kini, S. J. Jeon, D. K. Moon, *Adv. Mater.* **2020**, *32*, 1906175.

[68] L. Hong, H. Yao, Z. Wu, Y. Cui, T. Zhang, Y. Xu, R. Yu, Q. Liao, B. Gao, K. Xian, H. Y. Woo, Z. Ge, J. Hou, *Adv. Mater.* **2019**, *31*, 1903441.

[69] Y. Cui, H. Yao, L. Hong, T. Zhang, Y. Tang, B. Lin, K. Xian, B. Gao, C. An, P. Bi, W. Ma, J. Hou, *Natl. Sci. Rev.* **2020**, *7*, 1239.

[70] C. Sun, S. Qin, R. Wang, S. Chen, F. Pan, B. Qiu, Z. Shang, L. Meng, C. Zhang, M. Xiao, C. Yang, Y. Li, *J. Am. Chem. Soc.* **2020**, *142*, 1465.

[71] S. Li, C.-Z. Li, M. Shi, H. Chen, *ACS Energy Lett.* **2020**, *5*, 1554.